MONITORING HEAVY OIL RECOVERY BY TIME-LAPSE EEI INVERSION

NAIMEH RIAZI[1], LARRY LINES[1] and BRIAN RUSSELL[2]

[1] *Department of Geoscience, University of Calgary, Calgary, Alberta, Canada T2N 1N4. lrlines@ucalgary.ca*
[2] *Hampson-Russell Software, CGG, Calgary, Alberta, Canada T2P 2X6.*

(Received April 16, 2015; accepted May 14, 2015)

ABSTRACT

Riazi, N., Lines, L. and Russell, B., 2015. Monitoring heavy oil recovery by time-lapse EEI inversion. *Journal of Seismic Exploration*, 24: 343-364.

The application of time-lapse (4D) seismology in the monitoring and development of different oilfields has proven to be valuable in reservoir characterization. Time-lapse seismology utilizes successive seismic surveys acquired during the production of a reservoir in order to monitor production related changes by measuring the difference in elastic properties of subsurface. To monitor the reservoir related changes, rather than seismic processing and acquisition changes, a calibration process should be implemented to optimize and improve the repeatability of non-reservoir zones and consequently enhance the production-related anomalies in the reservoir. We can use two different approaches in our analysis, one based on seismic horizon changes and the other based on seismic volume changes. In time-lapse seismic horizon interpretation we measure the time-shift and amplitude differences along the seismic horizons both in the base and monitor surveys. In volume interpretation, we use seismic inversion, which incorporates time and amplitude changes in the reservoir, to derive impedance volumes and thus infer both pressure and fluid saturation changes. The elastic impedance (EI) inversion method proposed by Connolly (1999) is a technique used to extract elastic impedance volumes from partial angle-stack data, where elastic impedance is defined as the impedance that would be found by inverting linearized equation formulated by Aki and Richards (1980). Due to the variable scaling found at different incidence ray angles in the elastic impedance method, Whitcombe et al. (2002) normalized the technique and introduced a new technique called extended elastic impedance, or EEI, which uses the intercept and gradient volumes of standard AVO analysis as its seismic input rather than the angle-stack data, transformed using an angle (called chi) which correlates best with an elastic parameter of interest. Here, we apply both elastic impedance (EI) inversion and extended elastic impedance (EEI) inversion to time-lapse data acquired over a cold production heavy oilfield. We show which chi angles correlate best with our petrophysical attributes of interest. Furthermore, we illustrate how time-lapse EEI inversion results

asphaltenes, bitumens, pyrobitumens, resins, etc) compared to light oils (Batzle et al., 2006). Fig. 1, from Batzle et al., 2004 shows how Alaska heavy oil is different from the North Sea in composition. Note the spikes in the figure which indicate straight alkanes in the North Sea example. This is not seen in Alaska heavy oils due to biodegradation. Complex heavy oil components are left in the Alaska heavy oil samples rather than the alkanes in North Sea samples.

The viscosity of heavy oil is very high and can be changed by different factors such as pressure, gas content, temperature, and density. An increase in gravity (API) is correlated inversely with an increase in the viscosity of heavy oil. The viscosity in heavy oil dramatically decreases with increasing gas-oil ratio (GOR) and with temperature, and this is why the steam-based production recovery is very common for heavy oil. In addition to viscosity, other important elastic parameters decrease with increasing temperatures. This is because at low temperatures, heavy oil acts like a solid.

Seismic data has the advantage of being able to cover the entire reservoir volume whereas other techniques, such as well logging and core analysis, only cover the vicinity around the wellbore. In addition to those important advantages, seismic data can be used to track both static and dynamic properties

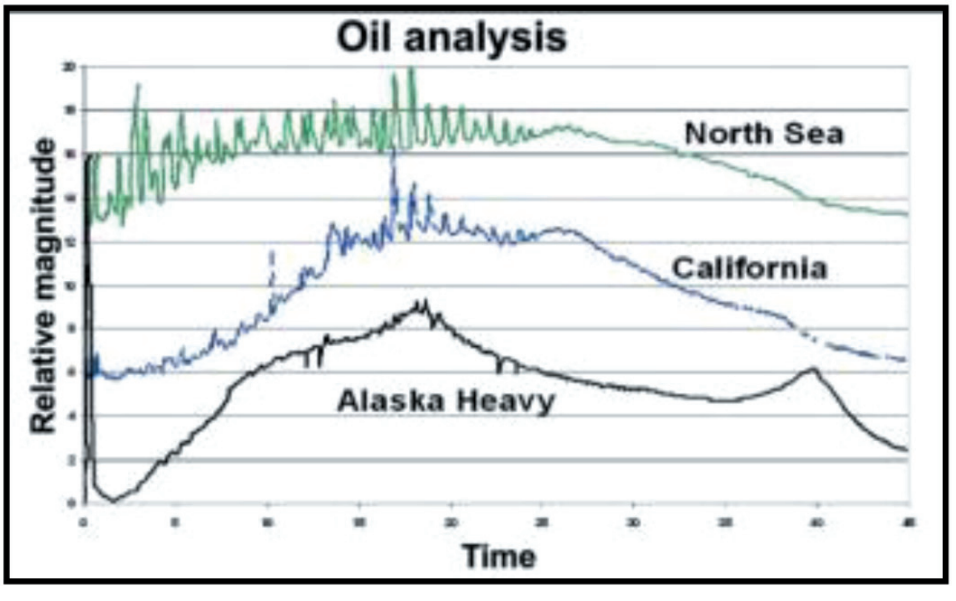

Fig. 1. Analysis of compositional tests on samples of North Sea, California and Alaska Heavy oil. The biodegradation effect on Alaska heavy oil samples are clear by removing the spikes seen in sample of North Sea (from Batzle et al., 2004).

of the entire reservoir by re-acquiring the data at different times during production, called the time-lapse, or 4D, seismology method. Time-lapse seismic studies have been used for the past two decades in many parts over the world, such as the North Sea, the Gulf of Mexico, and Canadian oil sands areas. Time-lapse seismology uses successive seismic surveys in a specified area to monitor the production-related changes. The application of time-lapse seismology has been shown to quantitatively measure the static and dynamic changes in a reservoir. Time-lapse seismology can thus be beneficial in understanding the fluid movement and stability of the reservoir.

Time-lapse time shifts, which are the time differences in one event observed in the base survey (the initial survey) as compared to the monitor survey (a subsequent survey), can be interpreted in order to understand the reservoir changes. The traveltime variation is used to monitor pore-pressure changes, stress changes, and compaction effects in the reservoir. Time-lapse seismic amplitude changes, which can be interpreted by using the amplitude versus offset (AVO) analysis technique, are also useful in time-lapse interpretation analysis.

The first time-lapse seismic survey was acquired in the mid-1980s in the Holt reservoir in the north central region of Texas. Greaves and Fulp (1987) discuss monitoring the propagation of an in-situ combustion (ISC) fire front in the Holt reservoir by time-lapse seismic analysis to improve the enhanced oil recovery (EOR) process. The in-situ combustion process was detected by three successive surveys which were acquired in the reservoir. This allowed an estimation of net burn volume to be made. The authors also proved that subtraction of base survey data (pre-burn) from monitor survey data (post-burn) produced results applicable in the monitoring the EOR process.

Time-lapse seismic analysis enables us to recognize the properties of hydrocarbon-producing reservoirs in 3-dimensional space during the time of production. This helps geoscientists and engineers to understand the in-situ status of the reservoir and find the ways to enhance the production in the remaining oil. The optimization process may not succeed without enough knowledge of the condition of the reservoir during hydrocarbon productions. Time-lapse seismic analyses are therefore important for the oil industry since the production and EOR monitoring using this approach is both low cost and high benefit.

The difference between the base and monitor surveys can be highly correlated with reservoir-related changes during the production. Since the time span between base and monitor surveys is normally short, we generally cannot attribute the differences in physical properties in the subsurface to the geological differences. However, care must be taken to distinguish production-related changes in the survey from non-production-related changes.

CASE STUDY

The studied heavy oilfield is located in the west central part of the province of Saskatchewan in Canada. The Sparky formation is prolific and is the target in this heavy oilfield. Well log data are available for several wells in this area and were used to build facies models in the area. Most of the wells in this area have density, gamma ray, and porosity logs. A few of the wells had P-wave logs, which were used in building the synthetic seismograms used in the time-lapse seismic analysis.

The recovery technique in this heavy oilfield is cold heavy oil production with sand (CHOPS). The cold production recovery process produces the heavy oil with sand, water and gas by the use of progressive cavity pumps without applying heat (Lines et al., 2008, Speight, 2009; Chopra et al., 2010). Cold heavy oil production with sand is one of major production recovery processes applied in heavy oil regions in western Canada. Fig. 2 illustrates various recovery techniques used in Alberta and Saskatchewan and also the location of the studied heavy oilfield. Simultaneous production of heavy oil and sand with CHOPS generates high porosity channels called wormholes (see Fig. 3). Wormholes can act like high permeability horizontal wells, which increases the production. The length of a wormhole can be up to 150 meters.

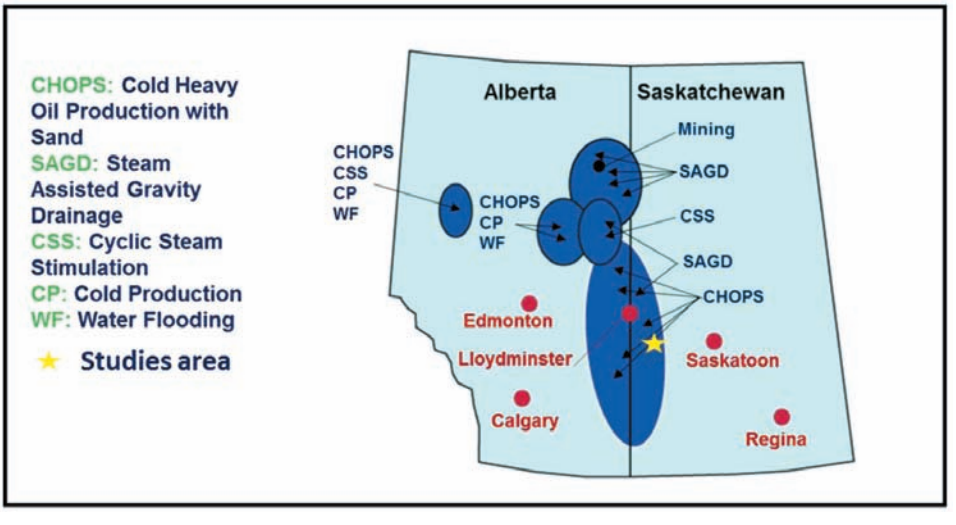

Fig. 2. Location of studied area and Types of recovery processes in Alberta and Saskatchewan associated with various oilfields (adapted from Hedlin et al., 2010).

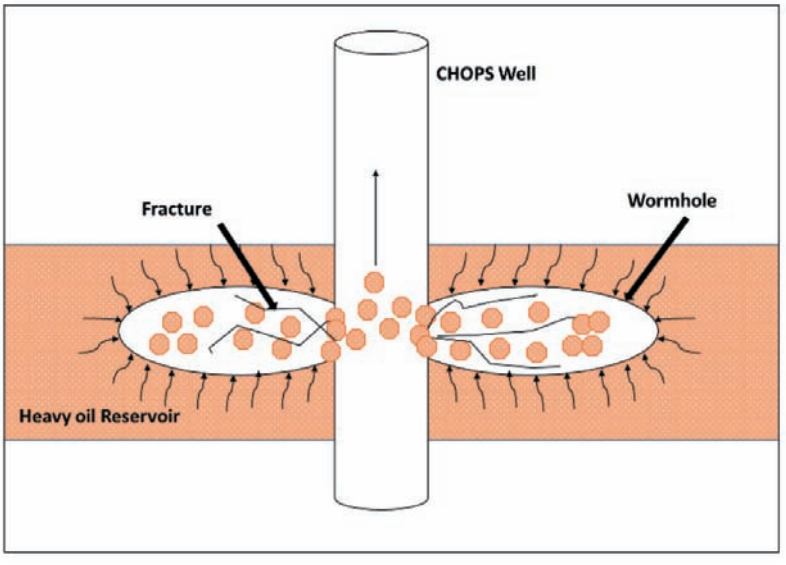

Fig. 3. Schematic mechanism in a CHOPS well (Riazi et al., 2014). The schematic has vertical exaggeration since the diameter of a wormhole can be as big as 10 cm but the extent of the wormhole network can be greater than 100 m.

As pressure declines in the reservoir due to production in heavy oil, pressure drops below bubble point pressure and gas comes out of solution producing what is called "foamy oil". The foamy oil can act like a gas-drive mechanism and increase the pressure within the reservoir to enhance the production recovery.

Understanding the properties of the reservoir rock is necessary for choosing the optimal cold production strategy (Speight, 2013). Therefore the need for recognizing the changes in the rock and fluid properties in the entire reservoir is essential for the success of the recovery processes. Time-lapse seismology can be a useful tool in monitoring the CHOPS process in order to optimize production.

The first 3D seismic survey covered a surface area of approximately 10.1 square kilometers in western Saskatchewan, east of the city of Lloydminster. The base survey was acquired in August 2003 and the second survey (the monitor survey) was acquired in January-February of 2009, both by Husky Energy. The base survey was processed through prestack time migration and the monitor survey was designed to record and mimic the offset limitations of the previous survey and was processed through the same steps. The base and monitor surveys were processed to produce zero-phase and normal polarity wavelets.

The reservoir is located between depths of 464 and 481 meters. The reservoir thickness is less than 10 meters. The porosity range in the reservoir is 18-38 % and the average horizontal permeability is up to 18 Darcies. The initial reservoir pressure at the shallowest depth was 3900 kPa.

TIME-LAPSE SEISMIC DATA PREPARATION

Consistent acquisition with the same source and receiver positions and identical methods of processing are difficult to obtain in time-lapse seismic studies. Correct and consistent acquisition and processing has an important role in the seismic data analysis, since this removes the non-production related anomalies in the seismic data and helps geophysicists to optimize the repeatability of the 4D seismic analysis. It also helps us to increase our confidence in the seismic analysis in the later steps.

Repeatability analysis has shown that even small changes in near-surface properties and acquisition parameters such as source and receiver positioning can have noticeable effects on time-lapse seismic results (Moldoveanu et al., 1996; Riazi and Lines, 2013). Near-surface geological effects and seasonal changes are other things which can affect the repeatability of 4D seismic surveys. It is necessary to remove these non-production effects, and this was done by using a processing technique known as cross-equalization. The cross-equalization process includes phase and time shifting, phase and frequency filtering, and cross-normalization to calibrate time-lapse seismic data. The first step involves applying phase and time shift equalization between the base and monitor surveys. By using phase and time shifting, we remove the anomalous amplitude and time differences above and below the reservoir zone that are not production related.

Applying a shaping filter between the base and monitor surveys is the next step. A full Wiener-Levinson transfer function including frequency-dependent phase as well as average power is applied, so that the wavelet is consistent between the two surveys. Cross-normalization of two surveys was done as the last step to compensate for amplitude changes caused by scaling. Fig. 4 compares the result of 4D calibration with the original data.

ROCK PHYSICS MODELLING

Before performing any time-lapse seismic analysis, rock physics modelling analysis should be performed. Here, we used Gassmann (1951) fluid substitution to model how the P-wave velocity changes with the saturation variation. The bulk modulus of saturated rock (K_{sat}) and shear modulus (μ_{sat}) can be estimated using the Gassmann equation, which is given by:

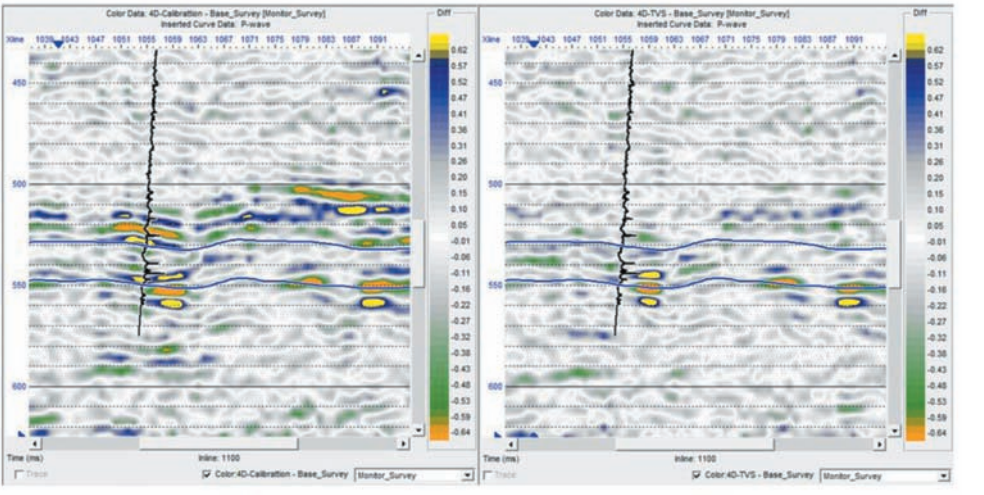

Fig. 4. Applying all the steps of 4D equalization, where a) shows the data before equalization and b) shows the data after equalization. The seismic traces are from base survey and color shows the difference between the monitor and base survey.

$$K_{sat} = K_{dry} + [1 - (K_{dry}/K_m)]^2/[(\phi/K_{fl}) + (1-\phi)/K_m + (K_{dry}/K_m^2)] \quad , \quad (1)$$

$$\mu_{sat} = \mu_{dry} \quad , \quad (2)$$

where ϕ is the porosity, K_{dry} is the bulk modulus of the dry porous frame of the rocks, μ_{dry} is the shear modulus of the dry porous frame of the rock, K_{fl} is the bulk modulus of the fluid and K_m is the bulk modulus of the mineral. The mineral bulk modulus can be modeled by Reuss-Voigt-Hill method by eq. (3):

$$K_m = \tfrac{1}{2}([V_{clay}K_{clay} + V_{qrz}K_{qrz}] + [V_{clay}/K_{clay} + V_{qrz}/K_{qrz}]^{-1}) \quad . \quad (3)$$

In eq. (3), V_{clay} and V_{qtz} are volume fractions of clay and quartz, respectively, and K_{clay} and K_{qtz} are the clay and quartz bulk moduli, respectively. The fluid modulus is given by the weighted harmonic average of the bulk moduli of the individual phases, which can be written as:

$$1/K_{fl} = (S_w/K_w) + (S_o/K_o) + (S_g/K_g) \quad , \quad (4)$$

where S_w, S_o and S_g are the water, oil and gas saturations, respectively, and K_w,

K_o and K_g are the water, oil and gas moduli, respectively. To model the heavy oil phase behavior, the bulk moduli of the various phases were obtained by using the equations of Batzle and Wang (1992), which are dependent on hydrocarbon temperature, API and GOR. Saturated P-wave and S-wave velocities can be estimated by

$$V_{P_{sat}} = \sqrt{\{[K_{sat} + (4/3)\mu_{sat}]/\rho_{sat}\}} \quad , \tag{5}$$

and

$$V_{S_{sat}} = \sqrt{\{\mu_{sat}/\rho_{sat}\}} \quad , \tag{6}$$

where $V_{P_{sat}}$ and $V_{S_{sat}}$ are the saturated P-wave and S-wave velocities, respectively. The shear modulus in eqs. (5) and (6) was computed by assuming that the ratio between the bulk and shear moduli of the dry rock is close to a value of one. Also, in the Gassmann equations, the shear modulus does not change for varying saturation at constant porosity. The density ρ_{sat} is found using the volume average equation given by

$$\rho_{sat} = \rho_m(1 - \phi) + \rho_w S_w \phi + \rho_{oil} S_{oil} \phi + \rho_{gas} S_{gas} \phi \quad . \tag{7}$$

Fig. 5 shows the modeling result when gas comes out of solution just by 10%, where the red and blue curves indicate the initial and target models before and after fluid substitution in the reservoir zone. The curves from left to right in Fig. 5 are the P-wave velocity, S-wave velocity, and density logs.

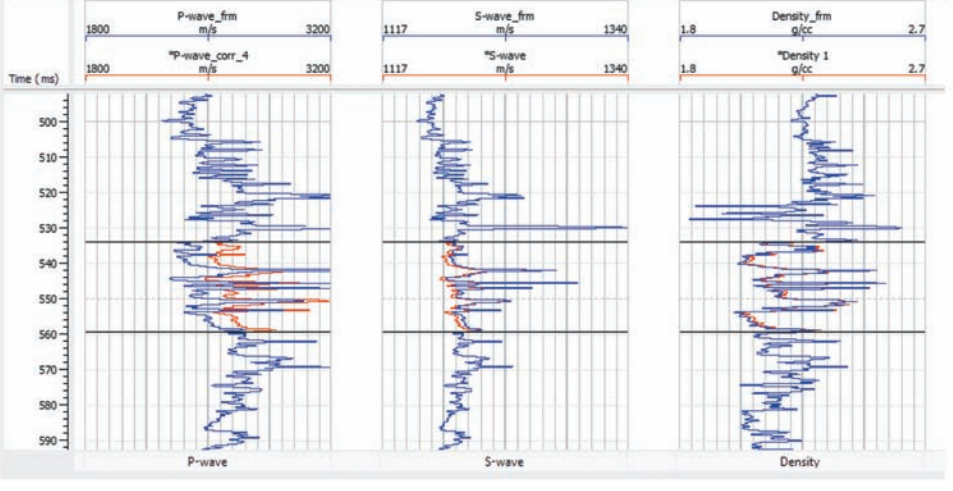

Fig. 5. The fluid substitution modeling results, where red shows the logs before fluid substitution and red shows the logs after fluid substitution. From left to right, the tracks represent the P-wave velocity, S-wave velocity, and density logs.

To understand the pressure effects on elastic properties of the unconsolidated heavy oil reservoir, we used Hertz-Mindlin modeling (Mindlin, 1949). Hertz-Mindlin equations [eqs. (8) and (9)] describe the elastic moduli of dry dense random pack of identical spherical grains at critical porosity (ϕ_0) in terms of the effective pressure (P), grain shear modulus (μ), and grain Poisson's ratio (ν) of the rock.

$$K_{HM} = \{[C^2(1 - \phi_0)^2\mu^2/18\pi^2(1 - \nu)^2]P\}^{1/3} \quad , \tag{8}$$

$$\mu_{HM} = [(5-4\nu)/5(2-\nu)]\{[3C^2(1 - \phi_0)^2\mu^2/2\pi^2(1 - \nu)^2]P\}^{1/3} \quad , \tag{9}$$

where C is the coordination number which is the average number of contacts per sphere.

Eqs. (8) and (9) are the elastic properties of sand at critical properties. In order to find the effective moduli at different porosity, Hashin-Shtrikman lower bound (Dvorkin and Nur, 1996) is used to describe the unconsolidated sand model as below:

$$K_{eff} = \{(\phi/\phi_0)/[K_{HM}+(4/3)\mu_{HM}] + [1-(\phi/\phi_0)]/[K+(4/3)\mu_{HM}]\}^{-1} - (4/3)\mu_{HM} \quad , \tag{10}$$

$$\mu_{eff} = \{(\phi/\phi_0)/[\mu_{HM}+(\mu_{HM}/6)\left((9K_{HM}+8\mu_{HM})/(K_{HM}+2\mu_{HM})\right)] + [1-(\phi/\phi_0)]/[\mu+(\mu_{HM}/6)\left((9K_{HM}+8\mu_{HM})/(K_{HM}+2\mu_{HM})\right)]\}^{-1} - (\mu_{HM}/6)\left((9K_{HM}+8\mu_{HM})/(K_{HM}+2\mu_{HM})\right) \quad , \tag{11}$$

where K and m are the bulk and shear modulus of the rock grain. Fig. 6 shows the effective bulk and shear modulus variation with pressure and porosity changes. It is obvious that the bulk modulus decreases by dropping the pressure in the reservoir.

TIME-LAPSE SEISMIC HORIZON INTERPRETATION

Changes in the amplitude strength can be caused by pressure reduction, fluid changes, and lithology and porosity variations during hydrocarbon production. When gas comes into the solution, we expect to see an increase in travel-time at the base of the reservoir due to the decrease of velocity in the reservoir during hydrocarbon production.

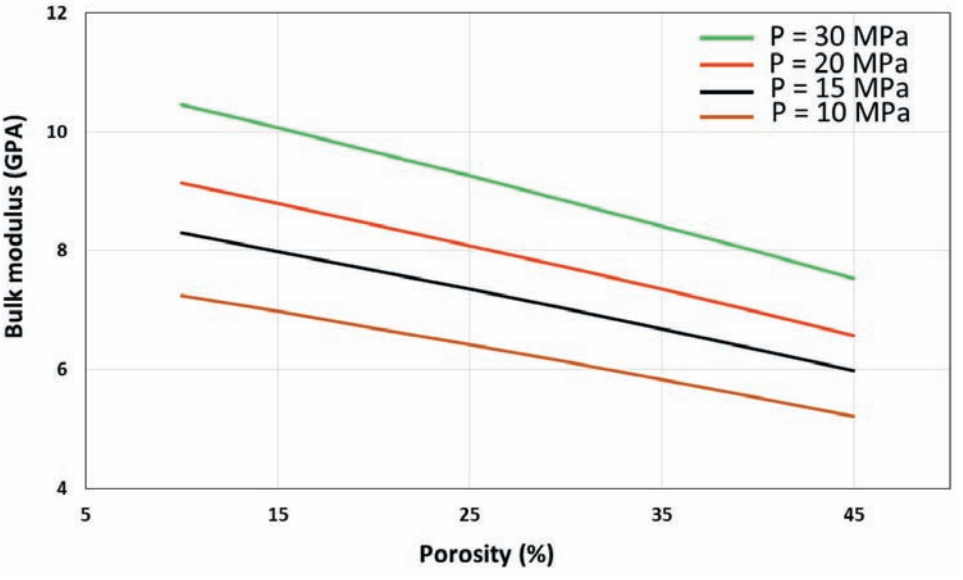

Fig. 6. A plot of bulk modulus changes with porosity. The highest pressure is the top curve, with the pressure decreasing downward for each curve.

First, the seismic-to-well tie was done for each well which had P-wave and density logs available in the dataset. Then, the seismic horizons from the top and base of the reservoir were interpreted on the base survey. The same horizons were interpreted in the monitor survey to allow us to analyze the time-shift and amplitude changes between the base and monitor surveys. Fig. 7 illustrates the time-shift and amplitude changes on the base-horizon between the base and monitor surveys. Both the time-shift and amplitude difference maps give significant information about the oil and gas production related changes observed in the reservoir. These changes are due to the saturation and pressure changes observed in the reservoir during the production time.

ELASTIC IMPEDANCE

Porosity, lithology and fluid changes in the reservoir can be interpreted from an analysis of the seismic amplitudes (Russell et al., 2006). This can be done through different techniques such as amplitude versus offset (AVO) analysis and post and pre-stack seismic inversion. AVO involves the analysis of the change in seismic reflectivity as function of offset and/or angle. The amplitude can be affected by variation in elastic properties of the subsurface strata, particularly P-wave velocity (V_P), S-wave velocity (V_S), and density (ρ).

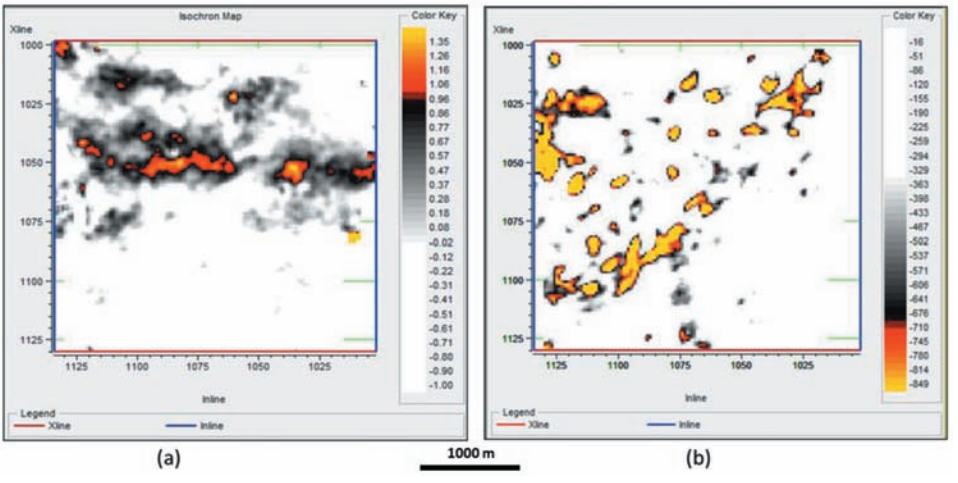

Fig. 7. Base reservoir horizon difference maps between the base and monitor surveys, where (a) shows the time change and (b) shows the amplitude change.

More fundamentally, changes in dynamic properties such as pressure and fluid saturation can alter the elastic properties of the reservoir and thus the amplitude of seismic reflectivity.

The basic assumption in post-stack seismic inversion is that the incidence angle for P-wave is normal and the variation of amplitude with offset cannot be determined. Thus, the only result from P-stack inversion is P-impedance. In fact, the stacked seismic trace is actually an average of the offset or angle gathers, and thus the stacked trace is not a true estimate of the normal incidence trace. On the other hand, utilizing the gathers themselves using the AVO technique provides more information about the reservoir since the AVO equations are based on gas-sensitive parameters such as V_P/V_S ratio and Poisson's ratio.

A well-known approach to AVO analysis is the intercept-gradient method which is based on the linearized formulation of the Zoeppritz equations by Aki and Richards (1980) and can be expressed as sum of three terms:

$$R_{PP}(\theta) = A + B\sin^2(\theta) + C\tan^2(\theta)\sin^2(\theta) \quad , \tag{12}$$

where A is the normal incident P-wave reflection coefficient $R_{PP}(\theta)$, B is the AVO gradient, and C is the curvature term. A, B, and C can be expressed in terms of V_P, V_S, and ρ changes as

$$A = \tfrac{1}{2}[(\Delta V_P/V_P) + (\Delta\rho/\rho)] \quad , \tag{13}$$

$$B = \tfrac{1}{2}(\Delta V_P/V_P) - 4[V_S/V_P]^2(\Delta V_S/V_S) - 2[V_S/V_P]^2(\Delta\rho/\rho) \quad , \tag{14}$$

and

$$C = \tfrac{1}{2}(\Delta V_P/V_P) \quad . \tag{15}$$

Note that V_P, V_S, and ρ are the average values between two layers across the interface for P-wave velocity, S-wave velocity, and density, respectively, and Δ is the operator giving the difference in velocity or density between two layers across the interface.

Connolly (2009) proposed the elastic impedance technique to generalize the acoustic impedance term for any angle of incidence in the partial angle-stacks.

$$EI = V_P^{(1+\tan^2(\theta))} V_S^{(-8K\sin^2(\theta))} \rho^{1-K\sin^2(\theta)} \quad , \tag{16}$$

where $K = (V_S/V_P)^2$ and normally can be considered as the average of the ratio, $(V_S/V_P)^2$ for an interval. Elastic impedance is a generalized form of acoustic impedance which can be derived for different angles of incidence. Acoustic impedance is equal to elastic impedance at normal incidence. To account for the fact that EI does not scale correctly at different angles of incidence, Whitcombe (2002) modified and normalized Connolly's elastic impedance equation by using the reference velocity and density constants (V_{P0}, V_{S0}, and ρ_0) averaged over a target interval to normalize the elastic values in the equation and thus introduce non-dimensionality into the Connolly equation:

$$EI(\theta) = V_{P0}\rho_0(V_P/V_{P0})^{(1+\tan^2(\theta))}(V_S/V_{S0})^{(-8K\sin^2(\theta))}(\rho/\rho_0)^{(1-K\sin^2(\theta))} \quad . \tag{17}$$

Whitcombe et al. (2002) proposed replacing $\sin^2(\theta)$ with $\tan(\chi)$ in the second term of the Shuey equation to create a new transform in which the A and B intercept terms could be rotated by the angle χ. The reflectivity was also multiplied by $\cos(\chi)$, and a scaled reflectivity R_S expressed as:

$$R = A + B\tan\chi = [A\cos(\chi) + B\sin(\chi)]/\cos(\chi) \quad , \tag{18}$$

$$R_S = R\cos(\chi) = A\cos(\chi) + B\sin(\chi) \quad . \tag{19}$$

Then, the elastic impedance equation replaced with the extended elastic impedance, or EEI equation, which is written as:

$$EEI(\chi) = V_{P0}\rho_0[(V_P/V_{P0})^p(V_S/V_{S0})^q(\rho/\rho_0)^r] \quad , \tag{20}$$

where

$$p = \cos(\chi) + \sin(\chi) \quad , \tag{21}$$

$$q = -8K\sin\chi \quad , \tag{22}$$

$$r = \cos(\chi) - 4K\sin(\chi) \quad . \tag{23}$$

The χ angle range is from $-90°$ to $+90°$. The χ angle can be chosen in a way that correlates with elastic properties such as bulk modulus, Lamé constants, shale volume, water saturation, and porosity. In EEI inversion, eq. (19) is used to create the starting model, and eq. (20) is used to create the seismic volume to be inverted.

APPLICATION TO REAL TIME-LAPSE SEISMIC DATA

Elastic impedance (EI) inversion will now be applied the reservoir zone. As mentioned in previous section, this technique is based on the three-term Aki-Richards approximation and is a function of angle of incidence. One of the difficulties in analyzing the elastic impedance inversion process is the restricted range of angle of incidence and rapid changes of elastic impedance at different angle of incidence. Here, we applied elastic impedance inversion to time-lapse seismic data in order to monitor the changes caused by hydrocarbon production and fluid changes in the target zone. To process the elastic impedance inversion, we first divided the total angle gather data to two sub-angle gathers. In the studied area, two angle gathers were made for both base and monitor surveys. The near angle gather range is 0-15 degrees and the far-angle gather is 15-30 degrees. Elastic impedance logs, from the wells which have dipole sonic logs, were made corresponding to the average angle of incident in each angle-gather. The angle gather is then converted to angle-stacks and, by using the interpreted horizons and extracted elastic impedance logs from available wells, a low frequency elastic impedance model was built separately for the partial angle stacks. Near and far angle-stacks were independently inverted to give elastic impedance cubes for near and far stacks. This procedure was repeated for the monitor survey to give the time-lapse seismic inversion. Fig. 8 shows the difference in near angle stack elastic impedance inversion and far angle stack elastic impedance inversion in a seismic line of volume. For better visual understanding, we removed the wiggle traces. The color key in Fig. 8 is the difference between the base and monitor surveys.

As mentioned in the previous section, Whitcombe et al. (2002) proposed the extended elastic impedance inversion (EEI) method to modify the elastic impedance inversion method introduced by Connolly (1999). The modified version of elastic impedance allows us to discriminate between the fluid discrimination and lithology prediction. Furthermore, the chi angle range is between $-90°$ to $+90°$. We applied the elastic impedance inversion to pre-stack

time-lapse seismic data on the studied heavy field. We used the total range of angle gather in EEI process. First of all, A and B, first two terms in the Aki-Richards equation should be derived by AVO intercept/gradient analysis both in base and monitor surveys on angle gathers in each surveys. In the next step, the best chi angle (χ) was determined in the reservoir zone. For this process, we used from two methods. In the first method, cross-correlation of EEI values from well data was compared with different petrophysical and elastic parameters such as P-wave velocity, S-wave velocity, acoustic impedance, shear impedance, bulk modulus (κ), shear modulus (μ), and the Lamé attributes. Whitcombe et al. (2002) proposed that the following values for chi angle correlated well with the attributes shown on the left:

$$\kappa \propto \mathrm{EEI}(\chi = 12.4^\circ) \ , \tag{24}$$

$$\lambda \propto \mathrm{EEI}(\chi = 19.8^\circ) \ , \tag{25}$$

$$\mu \propto \mathrm{EEI}(\chi = -51.3^\circ) \ . \tag{26}$$

In this case study, the chi angles that we computed are different from the chi angles shown above due to different rock physics relationships in our data. In our studied area, the values for the different elastic properties are expressed as shown in Table 1.

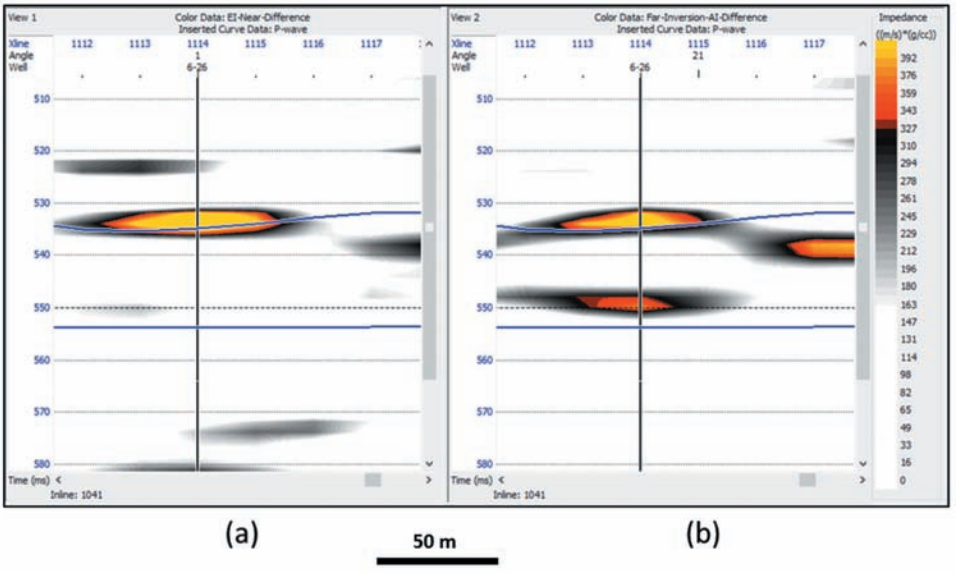

Fig. 8. A line from EI inversion Difference Volume, where a) is the near EI inversion, and b) is the far EI inversion.

Table 1. Correlation between seismic parameters and EEI chi angles.

Seismic parameters	EEI chi angle
κ	EEI ($\chi = 54°$)
λ	EEI ($\chi = 27°$)
V_P/V_S	EEI ($\chi = 45°$)
$\lambda\rho$ (Lamé attribute)	EEI ($\chi = 16°$)
$\mu\rho$ (Lamé attribute)	EEI ($\chi = -45°$)
μ	EEI ($\chi = -40°$)

Note that all the correlation coefficients for parameters given above are greater than 0.97.

To implement EEI inversion, the EEI reflectivity for the different chi angles was first derived from rotating the A and B volumes as in eq. (19). This procedure was repeated for the monitor survey. After extracting specific angle-stacks which corresponded to different EEI reflectivities and also defining a low-frequency elastic impedance model, inversion was done to derive EEI volumes for different chi angles. Fig. 9 shows an inverted seismic section of EEI ($\chi = 45°$) in the base and monitor seismic surveys. Fig. 10 illustrates the time-slice map of elastic impedance inside the reservoir for different chi angles which correlate with petrophysical parameters.

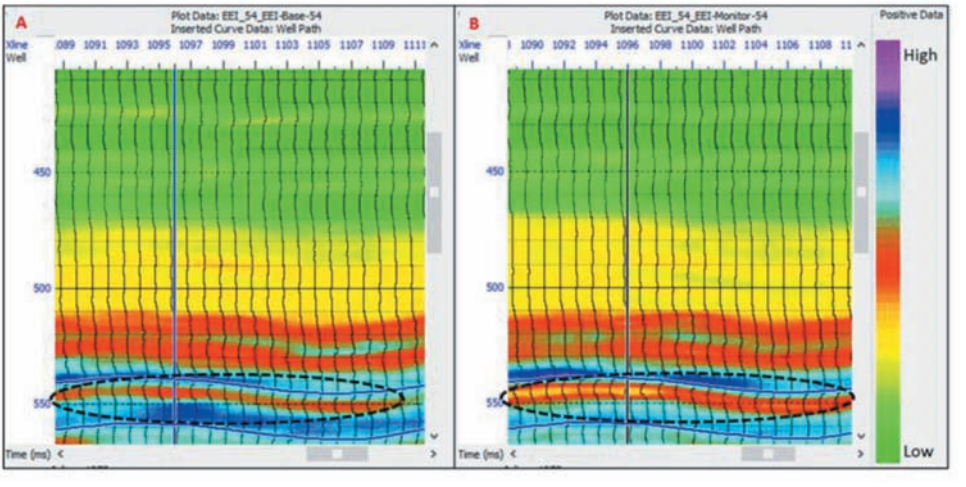

Fig. 9. A seismic section of EEI ($\chi = 45°$) in A) base survey B) monitor survey. The areas inside the ellipse is located at the reservoir zone, illustrate the changes during the production and recovery process.

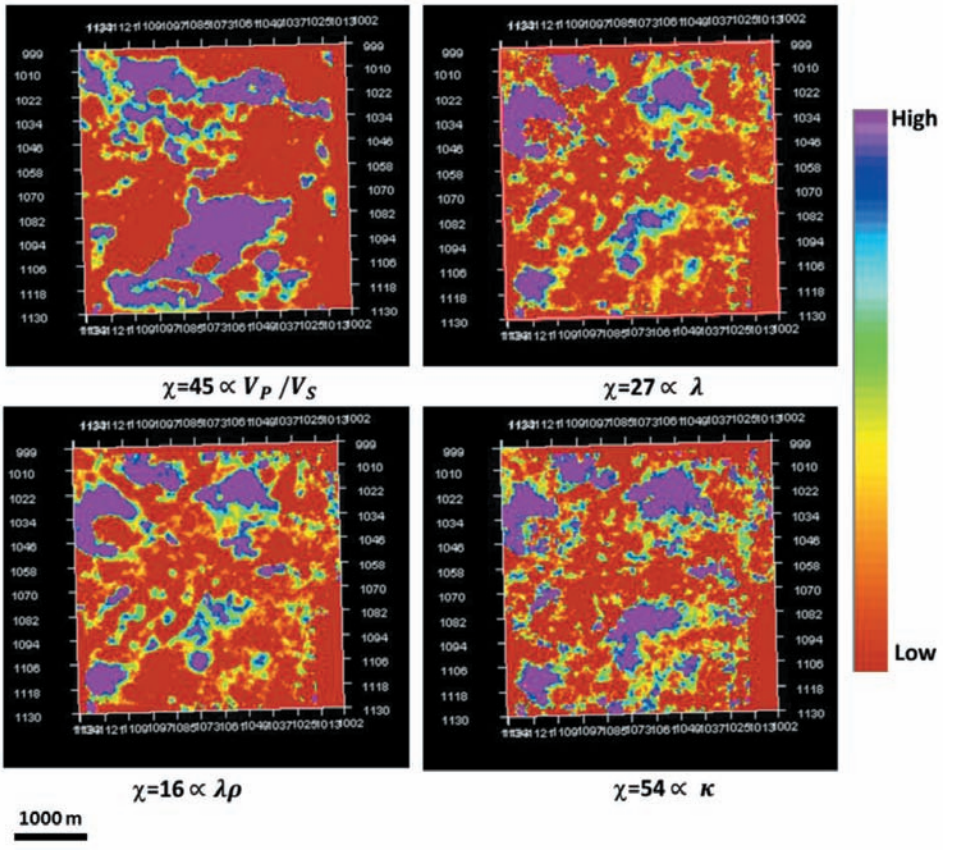

Fig. 10. Time-slice map of elastic impedance inside the reservoir for different chi angles which correlate with petrophysical parameters.

DISCUSSION

The integration of geology, geophysics, engineering and other related sciences is important to help in making a correct decisions field management of heavy oilfields. As shown in previous sections, two techniques of seismic inversion were applied to help in the interpretation of the cold production of heavy oil. Both EI and EEI inversions were used here to discriminate between the production-related zones. It is evident from these results that the outputs of EEI inversion are more promising since it shows higher changes close to CHOPS wells than EI inversion. They also show a larger anomalous area close to CHOPS wells. One of techniques which shows the quality of difference between two seismic parameters is normalized RMS (NRMS) method. NRMS technique computes the difference between two elements in the base and monitor surveys normalized by the average of the parameters in the base and monitor surveys. It can be defined as eq. (27):

$$NRMS = 200 \cdot RMS(m_t - b_t)/[RMS(m_t) + RMS(b_t)] \quad , \tag{27}$$

where m_t is the parameter from the monitor survey, and b_t is the corresponding parameter from the base survey. If we have no difference between base and monitor surveys, the NRMS value is 0. For a better comparison between the EI and EEI inversion results, NRMS maps are also made between the top and base of the reservoir. Fig. 11 shows the average map of elastic impedance volume in the reservoir zone for both near and far inversion. As illustrated in Fig. 11, time-lapse far elastic impedance inversion illustrates the changes in the reservoir zone better. The anomalous zones indicate 6% change in values of near and far inversion. Fig. 12 illustrates the NRMS maps of time-lapse EEI ($\chi = 45°$) and ($\chi = 27°$). As is evident in the figure, EEI ($\chi = 45°$) shows higher change (15%) in the production zone. However, EEI ($\chi = 27°$) shows the small production changes (3%) in the vicinity of the wells which their heavy oil production starts approximately in 2008 which is close to monitor seismic acquisition time at 2009.

Comparing the results of near and far time-lapse elastic impedance inversion (Fig. 11) with EEI results (Fig. 12), we can say that the far inversion EI output is similar to the EEI inversion results. This confirms the benefits of using high offset seismic surveys in reservoir characterization studies. However, these results are not completely consistent with the production changes in the studied area. They could not detect some of the important changes in the west of the studied area.

In Fig. 13, we compare the difference in the cumulative oil production with the results of the EEI inversions. In this figure, bubble size corresponds to the volume of cumulative oil production in the wells. Comparing the results of time-lapse EEI inversion (Fig. 14), we conclude that EEI ($\chi = 45°$), which correlates with V_P/V_S, distinctly discriminates between production-related and non-production zones.

Time-lapse seismic data can be an effective tool for infill drilling. Integration of time-lapse seismic analysis and reservoir engineering results can decrease the uncertainty in the development of heavy oilfields. That is because time-lapse seismic results provide information about the production related changes in the reservoir in the areas between the wells. We modelled the changes in elastic properties in well data by using Gassmann's method in the rock physics modeling part of this study. Fig. 14a shows how an EEI log can be changed by adding only 10 percent gas into the system. As is clear, the EEI ($\chi = 45°$) values decrease by gas input into the reservoir.

On the other hand, the low EEI values from the EEI inversion of the monitor survey are related to the high heavy oil accumulation in the reservoir. Furthermore, the hydrocarbon in the reservoir can be detected in the seismic

survey by decrease in the velocity and density (and hence the EEI values) compared to the surrounding rocks. Identifying these zones are possible in the EEI inverted volume at the monitor seismic time. These anomalous zones also coincide with the EEI difference (Fig. 12). Therefore, these zones can be considered as the target for the development of the field and new infill well drilling. By comparing the results of the time-lapse EEI ($\chi = 45°$) inversion for the monitor survey (Fig. 14b), we can observe that the areas which have higher production-related changes coincide with the areas of low EEI in the monitor survey. The areas shown by the ellipse correlate well with low EEI, possibly providing useful information for future drilling.

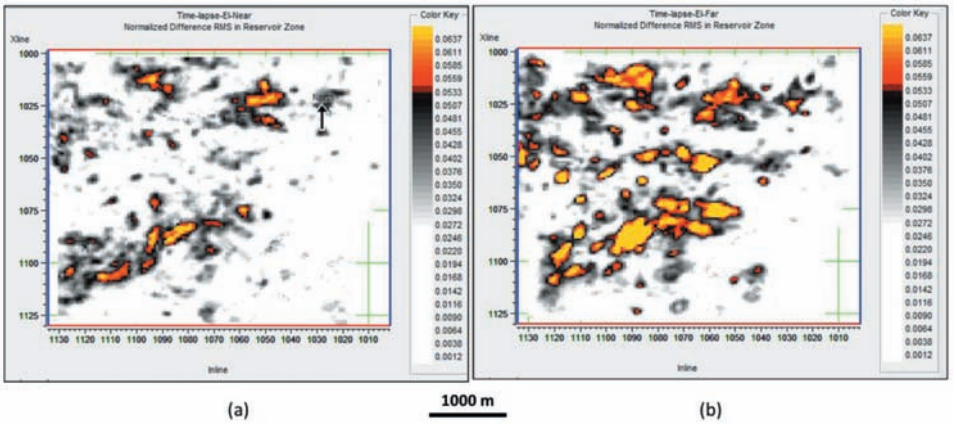

Fig. 11. Average map of EI inversion Difference in target zone, where a) near elastic impedance inversion, and b) far elastic impedance inversion.

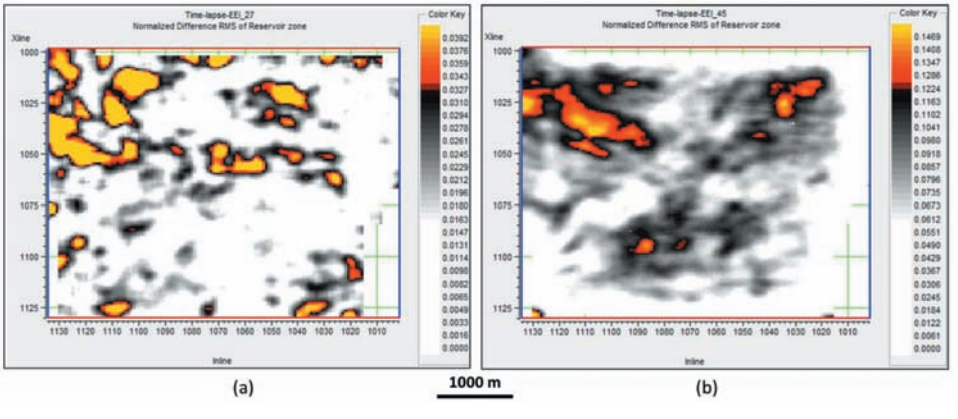

Fig. 12. NRMS map of time-lapse EEI inversion between the top and base of the reservoir for $\chi = 27°$ (left) and $\chi = 45°$ (right).

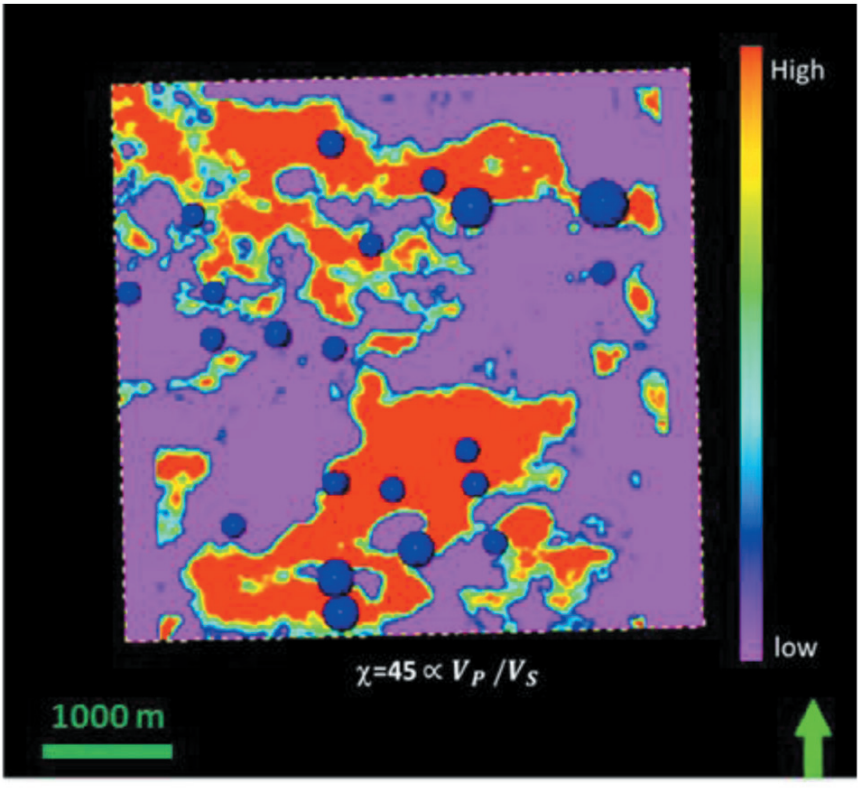

Fig. 13. Comparison of EEI ($\chi = 45°$) difference inversion with accumulative oil volume difference in the production time. Bubble size correlates with the volume of cumulative oil production between base and monitor surveys.

CONCLUSIONS

Time-lapse seismic analysis is a powerful technique for understanding fluid changes during the production of a reservoir. In this study, we applied elastic impedance inversion and extended elastic impedance inversion techniques to time-lapse seismic data acquired over a heavy oil field which was produced by the cold heavy oil production with sands (CHOPS) method. After briefly discussing heavy oils and their recovery method (especially the CHOPS method) and the geology and location of studied area, we discussed the important steps involved in the calibration of time lapse data, and showed how applying such a workflow helped us isolate amplitude change due to production which had occurred in the time interval between the base and monitor surveys over this field. In particular, a clear amplitude anomaly appeared when the base and monitor surveys were subtracted, indicating the presence of production related fluid change.

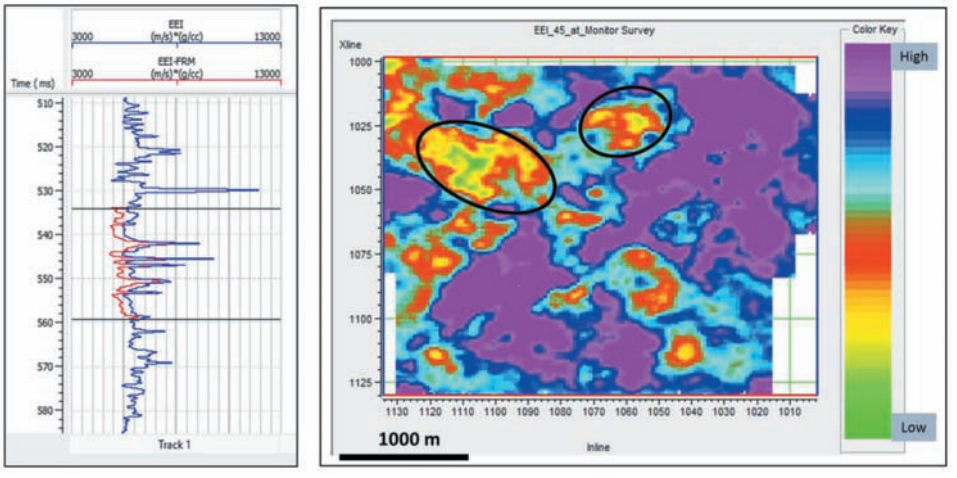

Fig. 14. a) Gassmann fluid substation modeling for EEI log, blue is original and red is target logs, b) average map of EEI ($\chi = 45°$) inversion in monitor surveys. Ellipse shows the areas of interest.

Before implementing time-lapse seismic inversion, we performed fluid replacement modelling using the Gassmann approach to help us link the reservoir properties and seismic data. By applying this rock physics model, we concluded that the elastic properties of the subsurface are affected by pressure and saturation changes during the heavy oil production. We found from Gassmann modelling that we would expect to see a reduction in the extended elastic impedance due to adding 10% gas to the reservoir. The Hertz-Mindlin model with a Hashin-Shtrikman lower bound was also used to model pressure changes. We illustrated that effective dry bulk and shear moduli can change due to pressure and saturation variation.

Comparing near and far EI inversion, it can be observed that far EI inversion identifies the anomalous zones in the reservoir better than EI near inversion (see Fig. 8 and Fig. 11). By analyzing the results of EI inversion and EEI inversion, we found that the Far EI inversion correlates roughly with the results of EEI inversion in detecting anomalous zones. However, EEI inversion for specific chi angles such as 45 degrees which corresponds with important seismic attributes such as V_P/V_S ratio and heavy oil production data demonstrates a higher rate of change (15%), especially close to the CHOPS wells. Therefore, EEI inversion is better able to detect small production related changes in the reservoir compared to EI inversion. Finally, we show that EEI inversion can be used as a key tool in the reservoir development plan and for making decisions about new infill drilling wells in the studied area.

ACKNOWLEDGMENTS

Authors would like to thank CHORUS sponsors for their financial support and software donations and Husky Energy Ltd. for providing the dataset for this study.

REFERENCES

Aki, K. and Richards, P.G., 1980. Quantitative Seismology. Freeman and Co., San Francisco.

Batzle, M. and Wang, Z., 1992. Seismic properties of pore fluid. Geophysics, 57: 1396-1408.

Batzle, M., Zadler, B., Hofmann, R. and Han, D.-H., 2004. Heavy oils - seismic properties. Expanded. Abstr., 74th Ann. Internat. SEG Mtg., Denver.

Batzle, M., Hofmann, R. and Han, D.-H., 2006. Heavy oils - seismic properties. The Leading Edge, 25: 750-756.

Chopra, S., Lines, L.R., Schmitt, D.R. and Batzle, M.L., 2010. Heavy Oils: Reservoir and Production Monitoring. Geophysical Developments, Vol. 13. SEG, Tulsa, OK.

Connolly, P.A., 1999. Elastic impedance. The Leading Edge, 18: 438-452.

Dusseault, M., 2002. Cold heavy oil production with sand in the Canadian heavy oil industry. Alberta Department of Energy Report.

Gardner, G.H.F., Gardner, L.W. and Gregory, A.R., 1974. Formation velocity and density - The diagnostic basics for stratigraphic traps. Geophysics, 39: 770-780.

Dvorkin, J. and Nur, A., 1996. Elasticity of high-porosity sandstones: Theory for two North Sea data sets. Geophysics, 61: 1363-1370.

Gassmann, F., 1951. Über die Elastizität Poröser Medien. Vierteljarhrsschr. Naturforsch. Gesellsch. Zür., 96: 1-23.

Greaves, R.J. and Fulp, T.J., 1987. Three-dimensional seismic monitoring of an enhanced oil recovery process. Geophysics, 52: 1175-1187.

Hedlin, K., Chan, A. and Godfrey, B., 2010. Time lapse interpretation of cold heavy oil production. CSEG Recorder, 35(7): 42-44.

Lines, L., Agharbarati, H., Daley, P.F., Embleton, J., Fay, M., Settari, T., Vasheghani, F., Wang, T. and Zhang, A., 2008. Collaborative methods in enhanced cold heavy oil production. The Leading Edge, 27: 1152-1156.

Moldoveanu, N., van Baaren, P., Addessi, D., Stubbington, L. and Combee, L., 1996. Repeatability of the seismic experiments for 4-D seismic in transition zone surveys. Expanded Abstr., 66th Ann. Internat. SEG Mtg., Denver: 5-8.

Riazi, N. and Lines, L., 2013. Reservoir characterization using time-lapse seismology over a cold production heavy oil reservoir. CSEG Recorder, 38(6): 40-47.

Riazi, N., Lines, L. and Russell, B., 2014. Cold heavy oil reservoir characterization by time-lapse seismic inversion, a case study. In: SPE Heavy Oil Conference - Canada. Paper No. 170127.

Russell, B., Hampson, D. and Bankhead, B., 2006. An inversion primer. CSEG Recorder, 31(2): 96-103.

Shuey, R.T., 1985. A simplification of the Zoeppritz equations. Geophysics, 50: 609-614.

Speight, J.G., 2013. Heavy Oil Production Processes. Gulf Professional Publishing, Houston.

Speight, J.G,, 2009. Enhanced Recovery Methods for Heavy Oil and Tar Sands. Gulf Publishing Co., Houston.

Whitcombe, D.N., 2002. Elastic impedance normalization. Geophysics, 67: 59-62.

Whitcombe, D.N., Connolly, P.A., Reagan, R.L. and Redshaw, T.C., 2002. Extended elastic impedance for fluid and lithology prediction. Geophysics, 67: 63-67.